catalysts

Highly Efficient and Magnetically Recyclable Non-noble Metal Fly Ash-based Catalysts for 4-Nitrophenol Reduction

Iwona Kuźniarska-Biernacka [1,*], Inês Ferreira [1], Marta Monteiro [1], Ana Cláudia Santos [2], Bruno Valentim [2], Alexandra Guedes [2], João H. Belo [3], João P. Araújo [3], Cristina Freire [1] and Andreia F. Peixoto [1,*]

[1] LAQV/REQUIMTE, Department of Chemistry and Biochemistry, Faculty of Science, University of Porto, Rua do Campo Alegre s/n, 4169-007 Porto, Portugal; up201704279@fc.up.pt (I.F.); acfreire@fc.up.pt (C.F.)
[2] Earth Science Institute—Porto Pole, Department of Geosciences, Environment and Spatial Plannings, Faculty of Sciences, University of Porto, Rua do Campo Alegre s/n, 4169-007 Porto, Portugal; anasantos@fc.up.pt (A.C.S.); bvvalent@fc.up.pt (B.V.); aguedes@fc.up.pt (A.G.)
[3] IFIMUP, Departamento de Física e Astronomia da Faculdade de Ciências da Universidade do Porto, Rua do Campo Alegre s/n, Porto 4169-007, Portugal; jbelo@fc.up.pt (J.H.B.); jearaujo@fc.up.pt (J.P.A.)
* Correspondence: iwonakb@fc.up.pt (I.K.-B.); andreia.peixoto@fc.up.pt (A.F.P.)

Table S1. Comparison of catalytic conditions and apparent first order rate constants for reduction of 4-NPh by FA_{mag}@CS@CuFe and similar catalytic systems recently reported.

Catalyst	mass[a] (mg)	V [b] (mL)	c_{4NPh}[c] (mg/mL)	$NaBH_4$[d] (mg)	*K1* (min^{-1})	ref
FA-Pd–Ag [f]	0.2	1.0	1.4×10^{-3}	37.0	0.7176	[54]
FA-Pd [f]	0.2	1.0	1.4×10^{-3}	37.0	0.5449	[54]
FA-Ag [f]	0.2	1.0	1.4×10^{-3}	37.0	0.5572	[54]
Au-PPy/FA [g]	1.0	8.6	9.7×10^{-2}	68.0	0.473	[55]
$CuFe_2O_4$/Ag@COF [h]	2.0	3.0	4.6×10^{-2}	3.4	0.77	[56]
$CuFe_2O_4$/Ag [h]	2.0	3.0	4.6×10^{-2}	3.4	0.25	[56]
$CuFe_2O_4$@COF [h]	2.0	3.0	4.6×10^{-2}	3.4	0.15	[56]
ESM/$CuFe_2O_4$ [i]	10.0	40.0	2.0×10^{-2}	0.05	0.748	[57]
$CuFe_2O_4$/CNC@Ag@ZIF-8 [j]	3.0	3.0	4.6×10^{-2}	3.4	0.64	[58]
$CuFe_2O_4$/CNC@Ag [j]	3.0	3.0	4.6×10^{-2}	3.4	0.25	[58]
$CuFe_2O_4$/CNC [j]	3.0	3.0	4.6×10^{-2}	3.4	0.08	[58]
98$CuFe_2O_4$-2RGO [k]	0.2	8.0	7.04×10^{-1}	7.56	0.48	[59]
96$CuFe_2O_4$-4RGO [k]	0.2	8.0	7.04×10^{-1}	7.56	1.032	[59]
94$CuFe_2O_4$-6RGO [k]	0.2	8.0	7.04×10^{-1}	7.56	0.618	[59]
92$CuFe_2O_4$-8RGO [k]	0.2	8.0	7.04×10^{-1}	7.56	0.588	[59]
C-dot@$CuFe_2O_4$ [l]	0.05	3.0	1.40×10^{-2}	9.45	4.0258	[60]
$CuFe_2O_4$-CDs [m]	0.05	3.0	1.70×10^{-2}	9.5	9.12	[61]
FA_{mag}@CS@CuFe	100	30	7.7	56.7	1.9761	This work

[a] catalysts mass; [b] volume total of the reaction mixture; [c] concentration of 4-NPh in the reaction mixture; [d] mass of $NaBH_4$ in the reaction mixture; [e] apparent first-order kinetic constant of reduction of 4-NPh; [f] FA-Pd-Ag - Coal Fly ash supported Pd–Ag bimetallic nanoparticles, FA-Pd- Coal Fly ash supported Pd nanoparticles, FA-Ag- Coal Fly ash supported Ag nanoparticles; [g] Au-PPy/FA - core-shell composite microspheres with fly ash (FA) and Au nanoparticles embedded in polypyrrole (PPy) chains; [h] $CuFe_2O_4$/Ag@COF - core-shell structure nanocomposite containing magnetic $CuFe_2O_4$/Ag nanoparticles and porous COF (covalent organic frameworks), where 1,3,5-tris(4-aminophenyl)benzene and 2,5-dimethoxyterephaldehyde, was utilized as the COF shell material; [i] ESM/$CuFe_2O_4$ - eggshell membrane-$CuFe_2O_4$ nanocomposite, the 4-NPh conversion 98.8% during 5.5 min; [j] $CuFe_2O_4$/CNC@Ag@ZIF-8 - cellulose nanocrystals (CNC) supported magnetic $CuFe_2O_4$@Ag@ZIF-8 nanospheres where ZIF-8 framework is $Zn(MeIM)_2$ where MeIM is 2-methylimidazole, $CuFe_2O_4$/CNC@Ag nanocomposite consisted of cellulose nanocrystals and $CuFe_2O_4$/Ag nanoparticles, $CuFe_2O_4$/CNC - cellulose nanocrystals supported $CuFe_2O_4$ nanoparticles; [k] 98$CuFe_2O_4$-2RGO -reduced graphene oxide (RGO) nanocomposite with 98 wt%$CuFe_2O_4$ and 2 wt% RGO, 96$CuFe_2O_4$-4RGO - nanocomposite with 96 wt%$CuFe_2O_4$ and 4 wt% RGO, 94$CuFe_2O_4$-6RGO - nanocomposite with 94 wt%$CuFe_2O_4$ and 6 wt% RGO, 92$CuFe_2O_4$-8RGO - nanocomposite with 92 wt%$CuFe_2O_4$ and 8 wt% RGO; [l] C-dot@$CuFe_2O_4$ - core–shell carbon dot@$CuFe_2O_4$ hybrid material; [m] $CuFe_2O_4$-CDs- Carbon dots coated $CuFe_2O_4$ nanocomposite

Figure S1. Detailed imaging and X-ray microanalysis of the FA_{mag}@CS@Cu sample

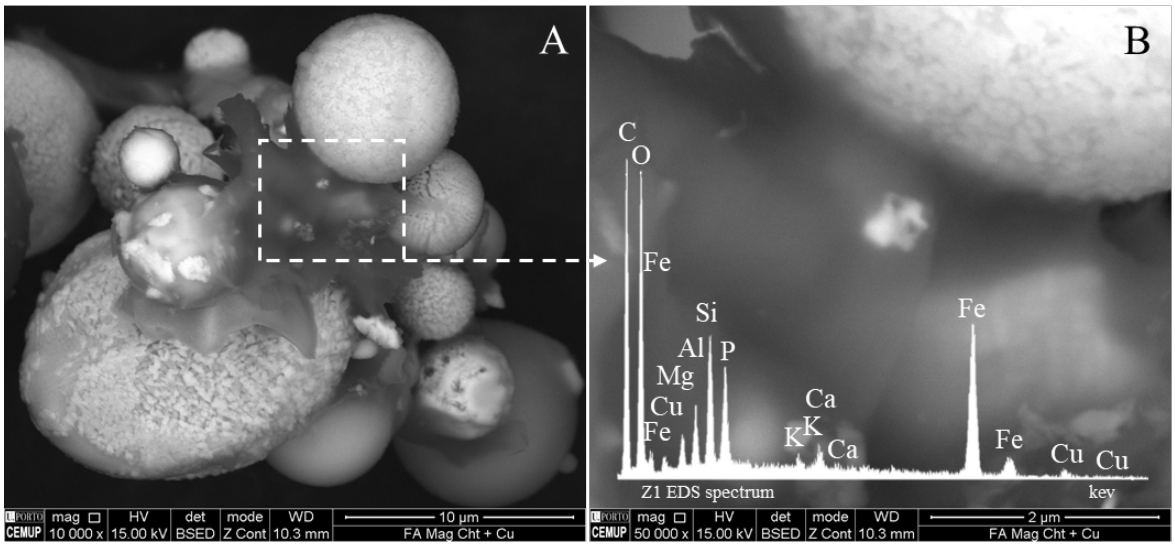

Figure S2. Elemental area-mappings for FA_{mag}@CS@Cu sample

FA_{mag}@CS@CuFe

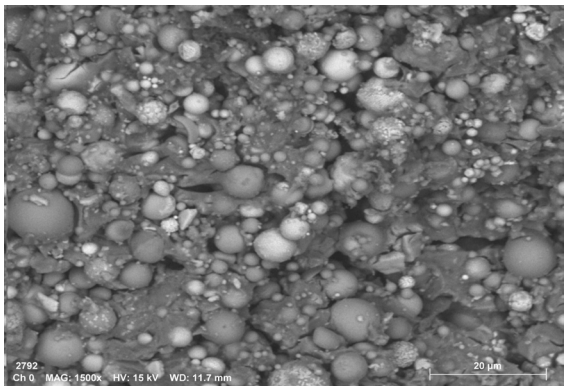

Carbon

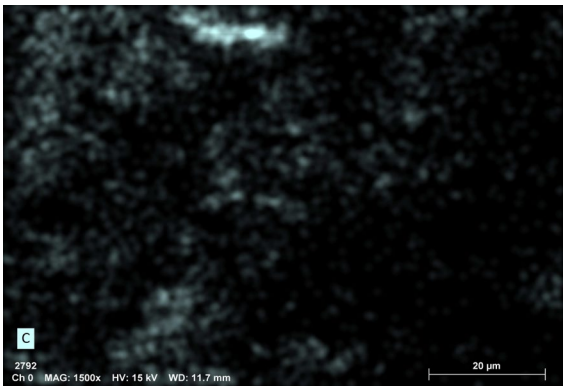

Iron

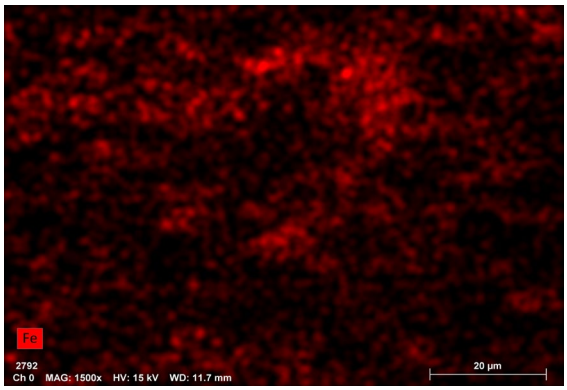

Copper

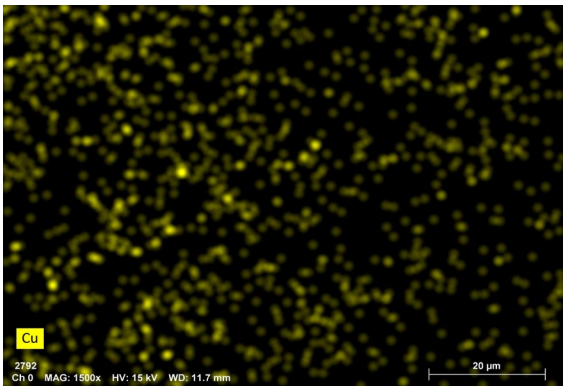

Figure S3. Change of UV–Vis spectrum of 4-NPh during the reduction of 4-NPh by $NaBH_4$ in the presence of: A - FA_{mag}@CS@CuFe, B - CuFe, C - FA_{mag}@CS@Cu, D - FA_{mag} and E - FA_{mag}@CS catalysts (initial 4-NPh concentration c = 5.5×10^{-5} M, catalyst dosage = 3.3 mg L^{-1}, $NaBH_4$ concentration c = 0.05 M).

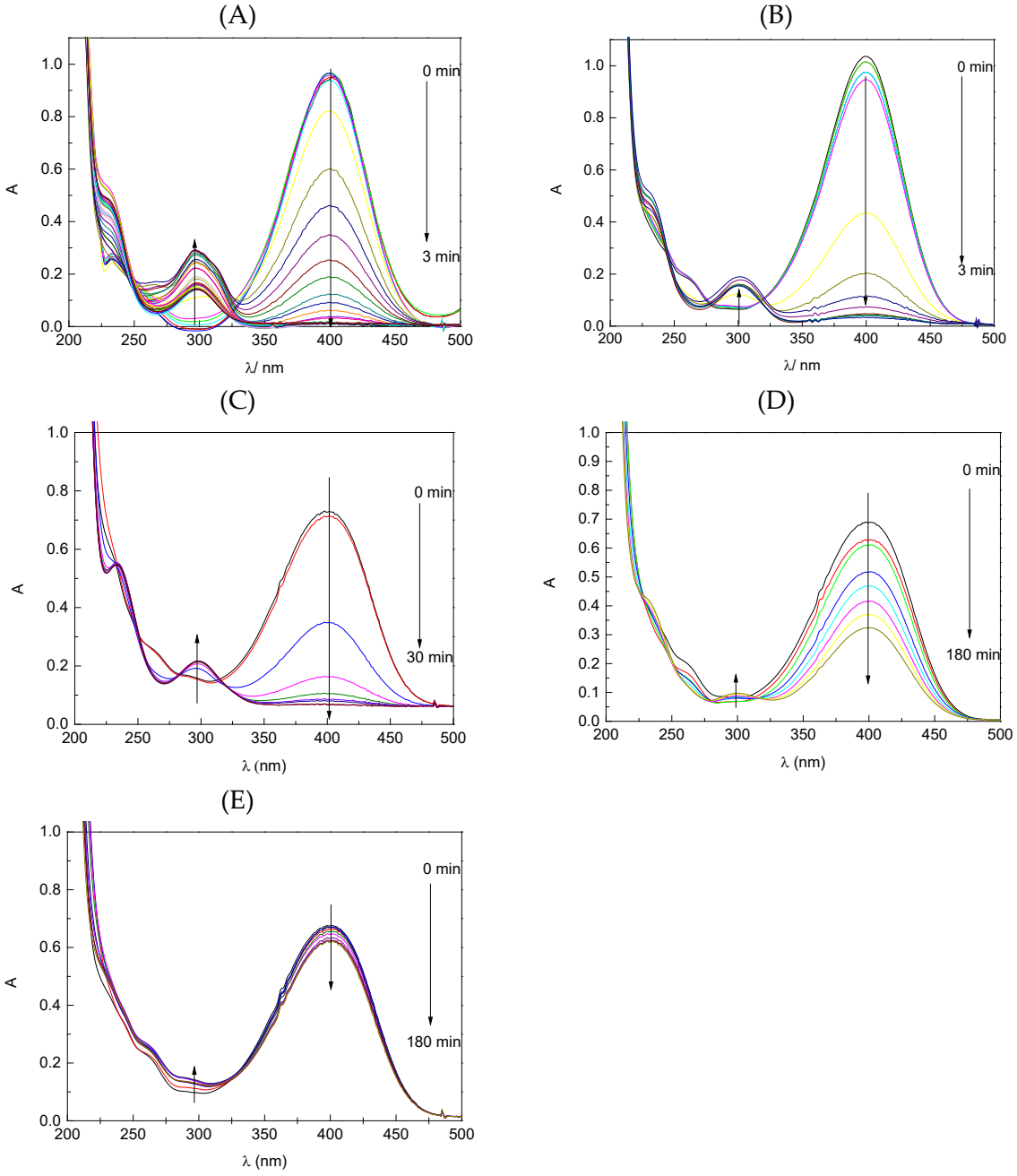

Figure S4. Reproducibility tests of FA_{mag} catalyst (initial 4-NPh concentration c = 5.5×10^{-5} M, catalyst dosage = 3.3 mg L^{-1}, $NaBH_4$ concentration c = 0.05 M).

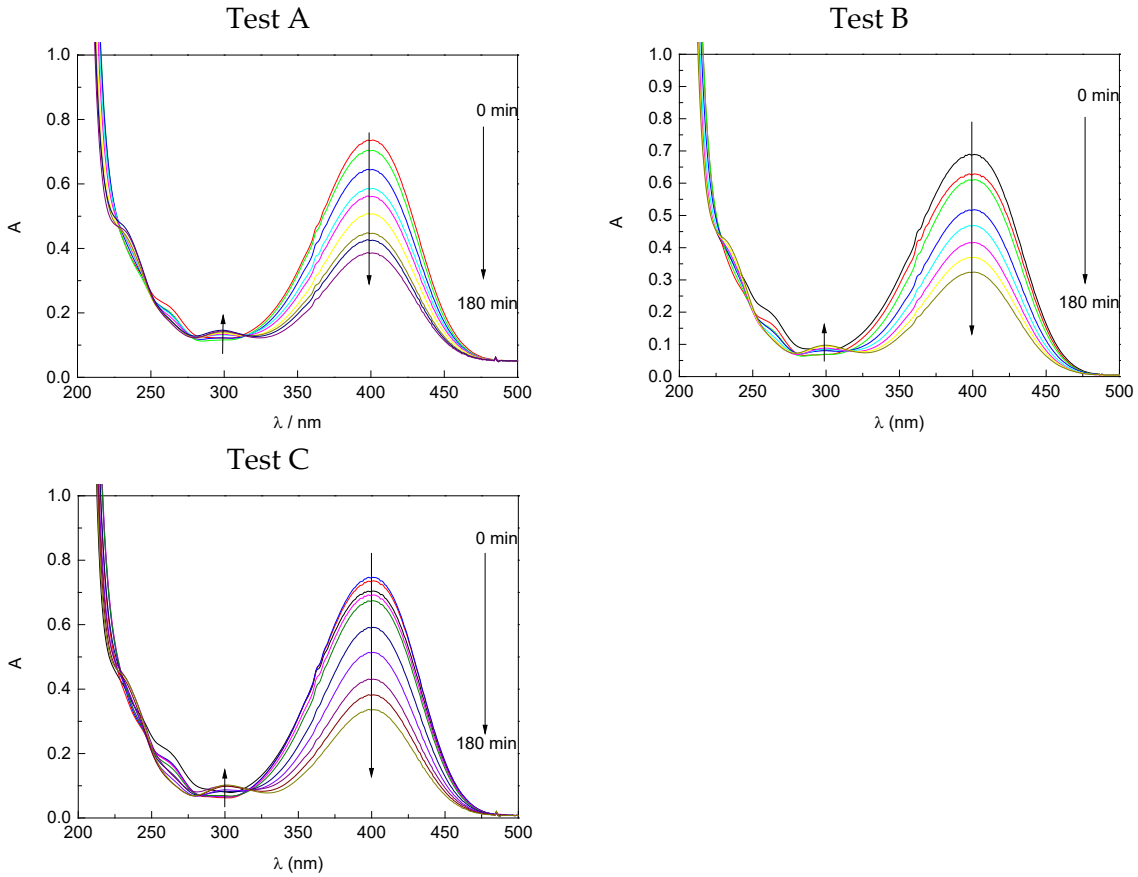

Figure S5. Stability tests of FA_{mag}@CS@CuFe catalyst (initial 4-NPh concentration c = 5.5×10^{-5} M, catalyst dosage = 3.3 mg L^{-1}, $NaBH_4$ concentration c = 0.05 M).

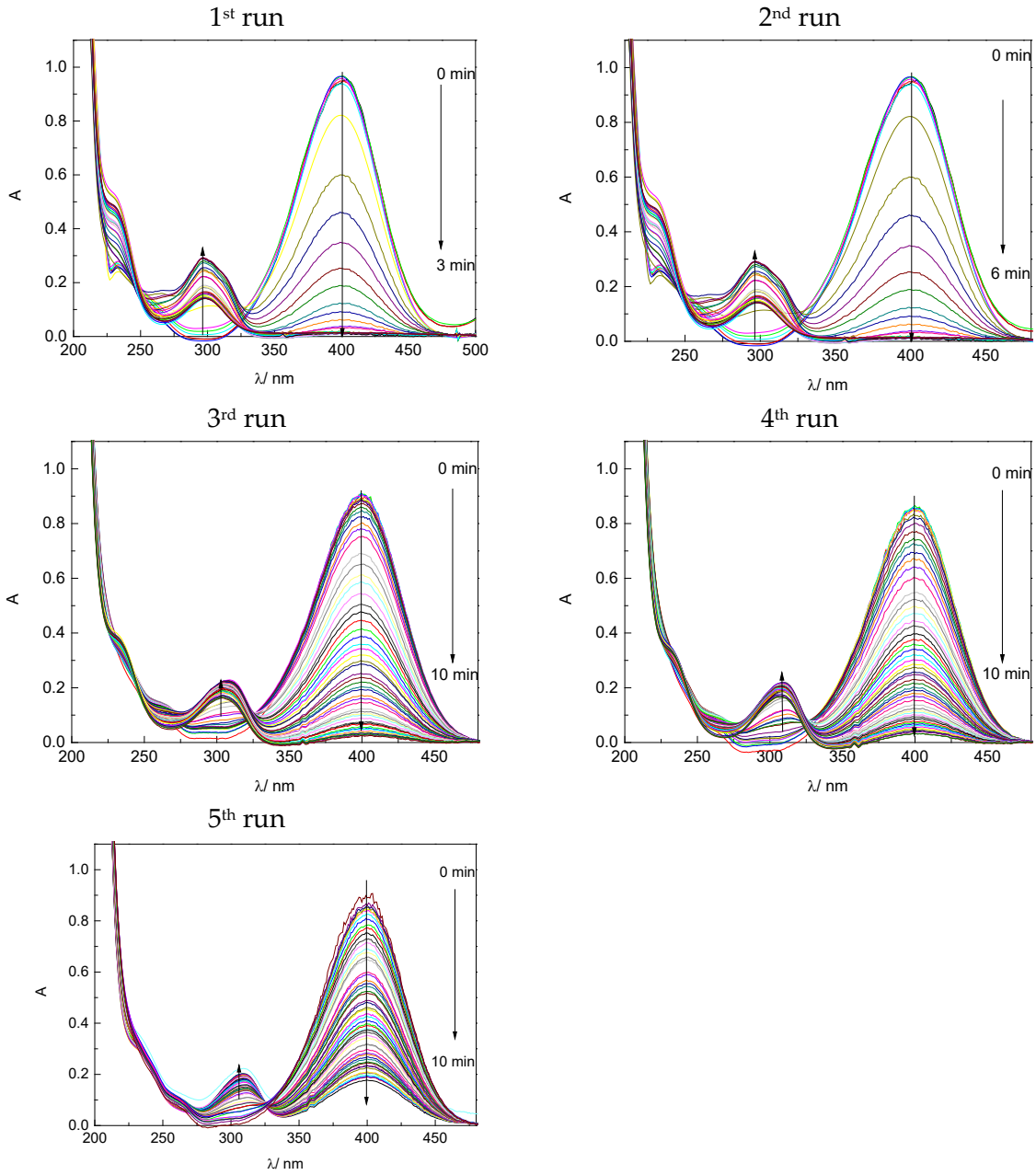

Figure S6. XRD patterns of CuFe nanoparticles, samples FA_{mag}, and composite FA_{mag}@CS@CuFe, where FA_{mag}@CS@CuFe* is the catalyst after the last catalytic cycle